Contents lists available at Science-Gate

International Journal of Advanced and Applied Sciences

Journal homepage: https://www.science-gate.com/IJAAS.html

Effect of organic matter on porosity changes in thermally treated oil shale based on the differential T_2 (DT_2) spectrum

Congming Ma, Bei Qiu, Lifeng Fan *

College of Architecture and Civil Engineering, Beijing University of Technology, Beijing 100124, China

ARTICLE INFO

Article history:
Received 14 May 2025
Received in revised form
26 October 2025
Accepted 24 December 2025

Keywords:
Oil shale
Organic matter
Nuclear magnetic resonance (NMR)
High-temperature treatment
Microstructural changes

ABSTRACT

Evaluating the porosity of oil shale at high temperatures is essential for resource exploration and development. However, the organic matter in oil shale rock, which is naturally rich in hydrogen, complicates assessments made using nuclear magnetic resonance (NMR) technology. In this paper, the differential T_2 (DT_2) spectrum method is introduced to correct the effects of organic matter on porosity measurements using nuclear magnetic resonance (NMR). Firstly, the T_2 spectrum was obtained for both dry oil shale rock, which contains organic matter, and saturated oil shale rock, which contains both organic matter and pore water. Secondly, the DT_2 spectrum of pore water in oil shale rock was obtained to determine the porosity of the oil shale rock containing organic matter. Finally, the impact of organic matter on the variation in porosity of oil shale rock as temperature increases was discussed. The results indicate that the porosity of oil shale rock increases slightly when the temperature is below 400 °C and rises significantly between 400 °C and 800 °C. The rate of porosity changes in oil shale rock increases gradually between 100 °C and 400 °C. The rate of porosity change in oil shale rock increases significantly and then decreases between 400 °C and 800 °C. There is a specific temperature at which the porosity changes of oil shale transitions from rapid to gradual.

1. Introduction

The production of shale oil through the pyrolysis of organic matter at high temperatures is influenced by the porosity of the oil shale rock (Saif et al., 2017; Burnham, 2017; Rabbani et al., 2017; Alrwashdeh, 2022). Therefore, it is essential to investigate the variation in porosity of thermally treated oil shale rock (Kang et al., 2020; Yang et al., 2019; Wang et al., 2019).

Various experimental methods have been employed to investigate the variation in porosity of dry rock and rock masses at elevated temperatures (Fan et al., 2020; Gautam et al., 2018; Wu et al., 2020; Zheng et al., 2022). The variation in the microstructure of rock during the thermal process is typically attributed to two primary causes. The primary cause is thermal stress resulting from the inhomogeneous expansion of mineral constituents, which leads to the initiation of micro-cracks when the stress exceeds the rock's strength (Rossi et al., 2018). The second cause is associated with mineral phase transitions in the rock, such as the transformation of α-quartz to β-quartz at approximately 573 °C, which generates trans-granular cracks and results in porosity variation in materials like granite (Feng et al., 2023; He et al., 2023; Yuan et al., 2022). To further explore the porosity changes in rock after thermal treatment, various laboratory technologies, such as X-ray computed tomography (CT) scans and gas adsorption, have been developed and frequently combined with digital image analysis methods (e.g., Digital Image Correlation or DIC) or other intelligent approaches to study the effects of high temperatures on porosity variations in rocks (Daigle and Johnson, 2016; Lei et al., 2021; Wang et al., 2021; Zhang et al., 2023).

In recent years, technologies have been developed to investigate the variation in porosity of rock and rock masses under saturated conditions at high temperatures, such as nuclear magnetic resonance (NMR) technology (Bi et al., 2023; Du et al., 2024). NMR technology measures the transverse relaxation time (T_2) of hydrogen atoms in water, and this measurement can be utilized to characterize the

* Corresponding Author.
Email Address: fanlifeng@bjut.edu.cn (L. Fan)
https://doi.org/10.21833/ijaas.2026.01.013
Corresponding author's ORCID profile:
https://orcid.org/0000-0002-7744-692X

volume of micro-defects in fully saturated rocks. NMR technology has been effectively utilized to study the porosity variations in thermally treated materials such as granite and sandstone, where only hydrogen atoms in pore water are present. However, for rocks that contain inherent hydrogen atoms, such as oil shale with organic matter, more complex methods are necessary. In these instances, two T_2 spectra can be obtained—one from organic matter and the other from saturated water (Lei et al., 2021; Zhan et al., 2022). Thus, it is essential to develop a new NMR method, such as the differential T_2 (DT_2) spectrum method, to minimize the interference caused by organic matter. While the DT_2 method is a known technique in NMR-based petrophysical analysis, its application to oil shale to correct hydrogen signal interference from organic matter is a significant and meaningful extension. It offers a unique perspective on understanding the effects of organic matter on porosity variation in thermally treated oil shale. Additionally, understanding the effects of organic matter on the variation of porosity in oil shale rock during or after exposure to high temperatures has significant implications for various applications.

In this study, the T_2 spectrum was obtained for both dry oil shale rock containing organic matter and saturated oil shale rock that includes both organic matter and pore water. The DT_2 spectrum of pore water in oil shale rock was obtained to determine the porosity of the oil shale rock containing organic matter. The impact of organic matter on the variation of porosity in oil shale rock as temperature increases was examined.

2. Samples and methods

2.1. Oil shale sample

Fig. 1a illustrates the oil shale sample obtained from the Songliao Basin in China (Feng et al., 2010). The Songliao Basin is one of the most significant hydrocarbon-bearing basins in the country, renowned for its substantial oil and gas resources (Tian et al., 2024). Recent studies have highlighted the basin's potential for large-scale unconventional oil production, with estimates suggesting vast in-place resources of shale oil. The samples were collected from the Nenjiang Formation at a depth of 1,800 meters underground. These samples were subsequently processed into cylindrical shapes with a diameter of 50.0 mm and a length of 25.0 mm, as illustrated in Fig. 1b.

Fig. 2 shows the mineral composition and corresponding proportions of the oil shale rock, as determined by X-ray diffraction (XRD) and scanning electron microscopy (SEM). Fig. 2a illustrates that the oil shale is composed of illite (36.31%), quartz (27.33%), illite/smectite (14.30%), feldspar (11.07%), pyrite (4.67%), and other minerals (6.32%). Fig. 2b illustrates the morphology of organic matter, which is observed as black and clustered among inorganic minerals. The organic matter in the oil shale from this region is sapropelic and demonstrates a high potential for hydrocarbon generation.

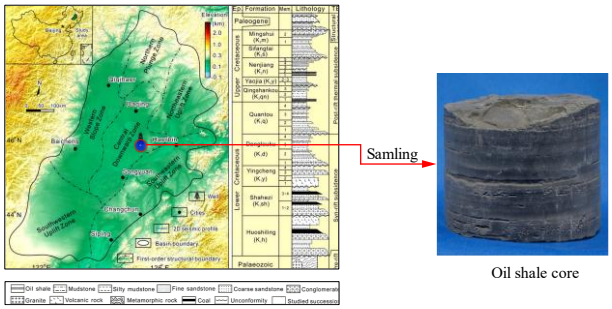

(a) Oil shale core

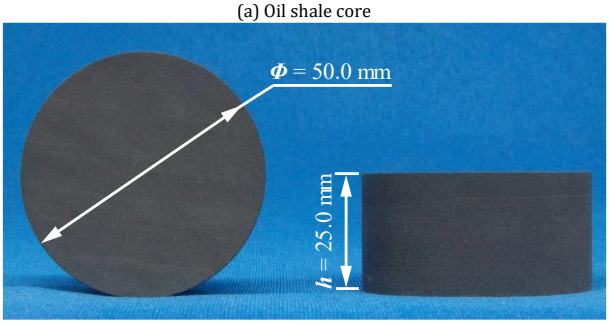

(b) Oil shale rock sample

Fig. 1: Oil shale rock sample from the Songliao Basin, China (Feng et al., 2010)

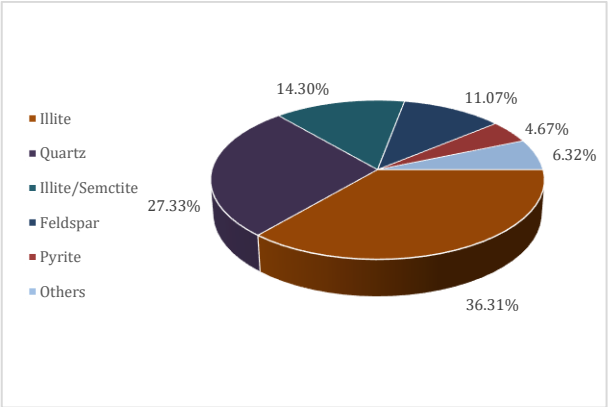

(a) Mineral components of oil shale rock

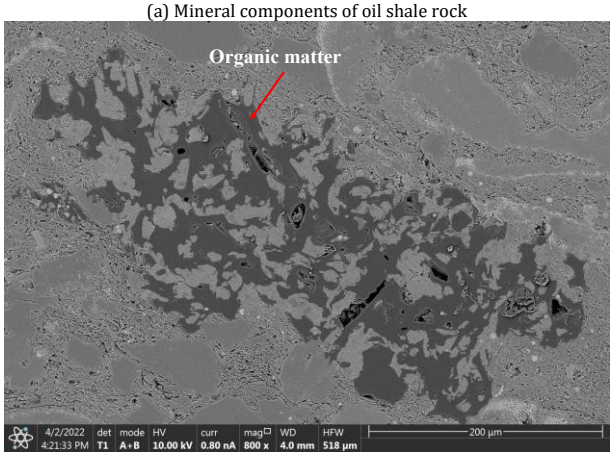

(b) Organic matter in oil shale rock

Fig. 2: Components of oil shale rock

2.2. Experimental design

For a single-phase hydrogen-containing substance, the T_2 spectrum obtained using NMR is the response characteristic of that phase of the

hydrogen-containing substance. But for rocks with multiphase hydrogen-containing substances, their signals of T_2 spectrum overlap (Li et al., 2020; Ma et al., 2020). When the pore structure of rock is measured by NMR technology, the T_2 spectrum of pore water is usually measured by filling with hydrogen-containing water. But oil shale itself contains hydrogen-rich organic matter. Therefore, it is necessary to use the differential T_2 (DT_2) spectrum method to distinguish pore water and organic matter.

Fig. 3 illustrates the experimental design for investigating the effects of organic matter on porosity variation in thermally treated oil shale, avoiding interference from hydrogen-rich organic matter. The experimental process can be divided into four stages: thermal treatment, the first NMR test, water-saturated treatment, and the second NMR test. Upon completing the experiments, the DT_2 spectrum method was used to obtain the T_2 spectra of pore water. It should be noted that in the calculation of the DT_2 spectrum, the two T_2 spectra are not directly calculated with a simple difference calculation. Specifically, the decay signals are first collected in thermal treatment and water-saturated state, the difference between the two decay signals is calculated, and then the T_2 spectrum of pore water is obtained by inversion (Ge et al., 2017). In this paper, the analysis software of the equipment is used to calculate the DT_2 spectrum. Then, the pore water T_2 spectra were used to determine the pore size distribution and porosity after correcting for the effect of organic matter. The thermal effect on the microstructural deterioration of oil shale was analyzed by examining the porosity change rate.

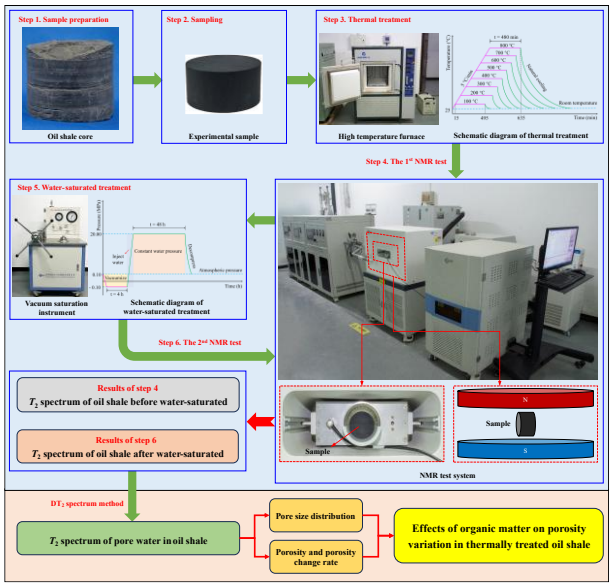

Fig. 3: Experimental design

2.2.1. Thermal treatment

Thermal treatments were performed using the SG-XL1200 high-temperature furnace. During the thermal treatments, a total of eight temperature levels were established: 100 °C, 200 °C, 300 °C, 400 °C, 500 °C, 600 °C, 700 °C, and 800 °C. Different samples were heated individually to their specified temperatures. The heating rate was maintained at 5.0 °C/min to prevent the effects of thermal shock (Saif et al., 2017; Fan et al., 2020). Upon reaching the specified temperatures, the samples were maintained for 8.0 hours before being cooled to room temperature.

2.2.2. NMR test

The NMR tests were conducted on samples using the Niumag MesoMR 14-060-I LF-NMR system. The resonance frequency was 12.00 MHz, and the diameter of the probe coil was 60.00 mm. The Carr-Purcell-Meiboom-Gill (CPMG) sequence was employed to evaluate the T_2 spectrum, using an echo time of 0.10 ms and a waiting time of 3000.00 ms (Li et al., 2020). Furthermore, the Half-Fourier acquisition single-shot turbo spin echo imaging sequence was utilized for nuclear magnetic resonance imaging (MRI) testing, featuring a repetition time of 300.00 ms and an echo time of 4.53 ms.

2.2.3. Water-saturated treatment

Water-saturated treatments were conducted on thermally treated samples using the ZYB-Ⅱ vacuum pressurization saturation device. Distilled water was used for saturation. During the water-saturated treatments, the oil shale rocks were initially subjected to vacuum for 4.0 hours in an environment with a pressure of -0.10 MPa. They were then submerged in water for 48.0 hours at a pressure of 20.00 MPa.

3. Results

3.1. Oil shale rock following thermal treatment

Fig. 4 illustrates the variation in the appearance of oil shale rock at different temperatures. The apparent color of oil shale remains predominantly black at temperatures 100 °C to 300 °C. Subsequently, it transitions from black to dark gray between 300 °C and 400 °C. Further heating results in a gradual transition in apparent color from dark gray to light gray between 400 °C and 600 °C. Finally, at 700 °C to 800 °C, the apparent color changes from light gray to pale yellow. Additionally, elevated temperatures lead to the formation of thermal cracks, including prominent surface cracks observed at 700 °C and 800 °C. Moreover, the observed crack propagation is aligned parallel to the bedding direction.

3.2. MRI of saturated oil shale rock

Fig. 5 illustrates the results of the MRI conducted at various temperatures on a cross-sectional scan area that encompasses the entire rock under water-

saturated conditions, where hydrogen signals originate from both organic matter and pore water. The red area gradually expands, indicating a progressive increase in the signal intensity of hydrogen atoms. This indicates an augmentation in both water content and pore quantity within the oil shale. The presence of ribbon-like red regions was observed at 700 °C and 800 °C. The hydrogen signal in this region is attributed to the presence of water in the cracks, with a higher concentration of water being detected. To summarize, the MRI results indicate that high temperature leads to the formation of pores in oil shale rock and promotes the expansion of fractures from a macroscopic perspective.

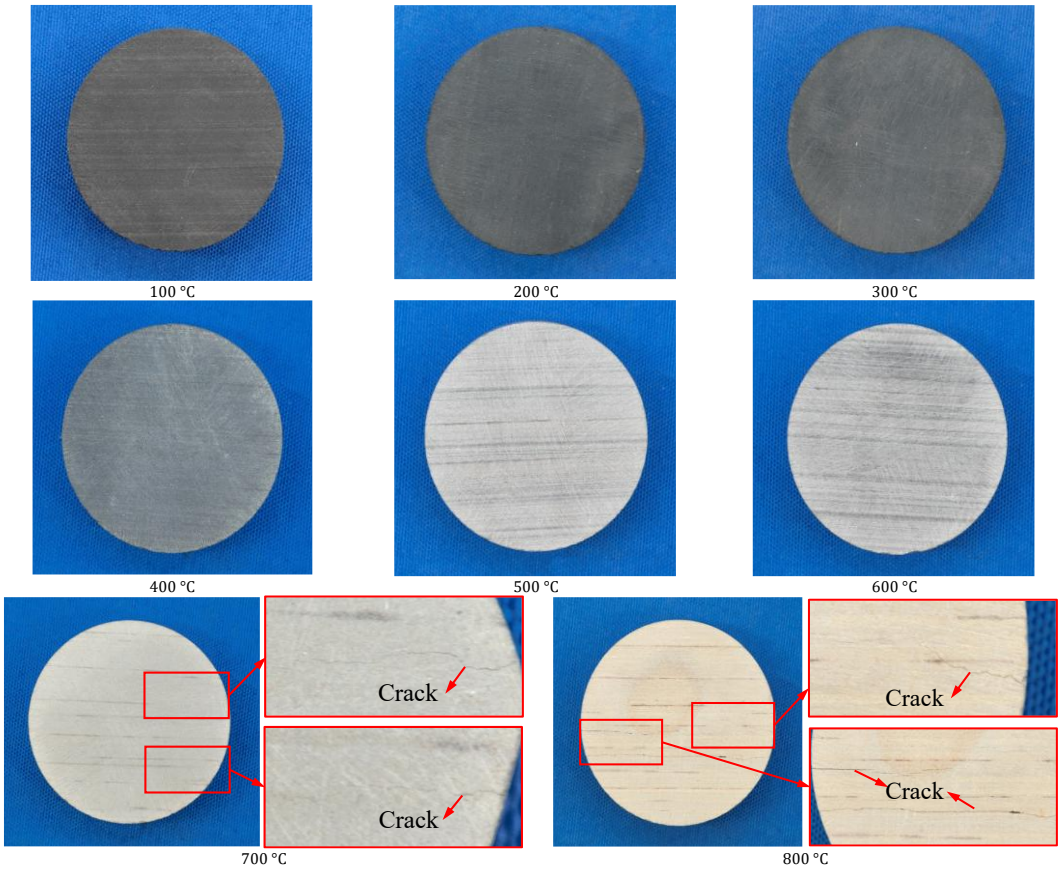

Fig. 4: Appearance variation of oil shale rock after thermal treatment

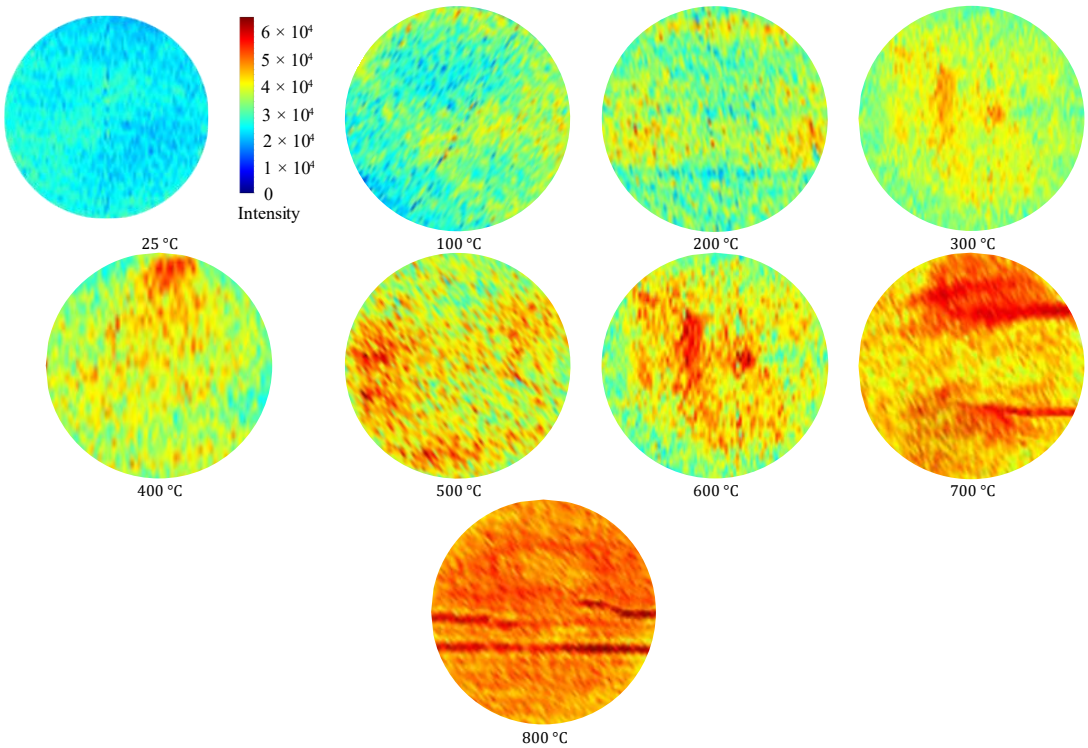

Fig. 5: Oil shale rock after thermal treatment

3.3. T_2 spectrum of organic matter and pore water in oil shale rock

Fig. 6 illustrates the T_2 spectrum of organic matter in oil shale rock. The T_2 spectrum exhibits two peaks at 25 °C, while at 100 °C, it displays only one peak. Additionally, there is a decrease in the T_2 spectrum area from 6.46 × 10^3 a.u. The value decreased to 4.08 × 10^3 a.u., representing a decrease of 36.81%. This decrease in hydrogen signal intensity observed in oil shale at this temperature may be attributed to the volatilization of water and oil present within the rock matrix. The curve subsequently displays an additional downward shift between 100 °C and 200 °C. The T_2 spectrum area experiences a decrease from 4.08 × 10^3 a.u. to 3.37 × 10^3 a.u. with a decrease of 17.47%. The curve remains relatively stable between 200 °C and 400 °C, and the T_2 spectrum area exhibits a decrease from 3.37 × 10^3 a.u. to 3.06 × 10^3 a.u., which corresponds to a decrease of 9.24%. Subsequently, at 400 °C and 500 °C, the curve shifts downwards, and the T_2 spectrum area decreases significantly from 3.06 × 10^3 a.u. to 1.41 × 10^3 a.u., indicating a substantial reduction of approximately 53.79%. This change further indicates that organic matter in oil shale rock may be significantly decomposed between 400 °C and 500 °C. Moreover, at temperatures of 500 °C and 600 °C, there is a further decrease in the T_2 spectrum area from 1.41 × 10^3 a.u. to 0.83 × 10^3 a.u. The percentage drop of 41.19%. Notably, when temperature is 600 °C, 700 °C, and 800 °C, the T_2 spectrum areas are measured as 0.62 × 10^3a.u., 0.37 × 10^3a.u., and 0.2 × 10^3 a.u. with a further decrease.

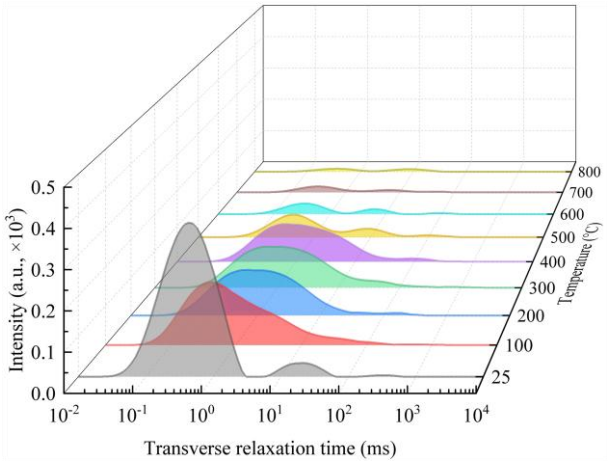

Fig. 6: T_2 spectra of organic matter

Fig. 7 illustrates the T_2 spectrum of organic matter and pore water in oil shale rock. At 25 °C to 100 °C, the area of the T_2 spectrum increases from 1.61 × 10^3 a.u. to 1.97 × 10^3 a.u. with an increase of 22.58%. At temperatures ranging from 200 °C to 400 °C, the T_2 spectrum area gradually increases, and it is 2.08 × 10^3 a.u. (200 °C), 2.25 × 10^3 a.u. (300 °C), and 2.26 × 10^3 a.u. (400 °C), respectively. At 500 °C, the T_2 spectrum area increases to 2.56 × 10^3 a.u. with an increase of 12.89% compared with 400 °C. The T_2 spectrum area increases from 2.56 × 10^3 a.u. to 2.86 × 10^3 a.u. at temperatures ranging from 500 °C to 600 °C, an increase of 12.20%. At 700 °C, the area of the T_2 spectrum increases obviously to 4.69 × 10^3 a.u., an increase of 64.06%. At 800 °C, the T_2 spectrum area continues to increase, reaching 5.08 × 10^3 a.u.. The above experimental phenomena show that after thermal treatment, the hydrogen signal of hydrogen-containing substances in oil shale under water-saturated states increases with the temperature increase, and this phenomenon is more significant between 600 °C and 700 °C.

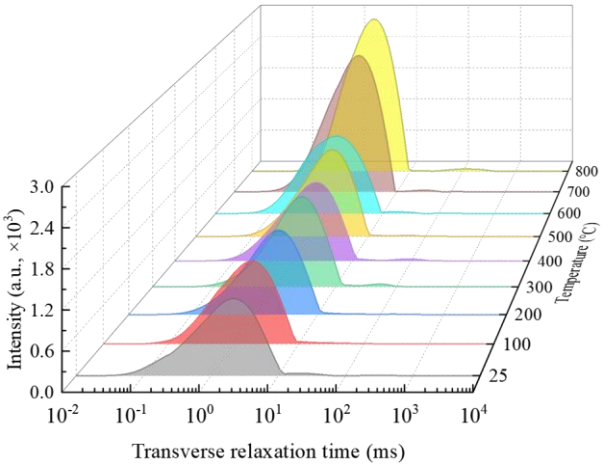

Fig. 7: T_2 spectra of organic matter and pore water

3.4. DT_2 spectrum of pore water in oil shale rock

Fig. 8 presents the DT_2 spectrum of pore water in oil shale rock, derived from the difference between Fig. 6 and Fig. 7. The T_2 spectrum area increases from 1.97 × 10^3 a.u. to 2.10 × 10^3 a.u. at 100 °C to 200 °C, there is an increase of 6.66%. The T_2 spectrum area increases from 2.10 × 10^3 a.u. to 2.25 × 10^3 a.u. at 200 °C to 300 °C, there is an increase of 6.93%. Between 300 °C and 400 °C, the curve shifts upwards, and the T_2 spectrum area increases from 2.25 × 10^3 a.u. to 2.26 × 10^3 a.u. with an increase of 0.53%. Between 400 °C and 500 °C, the curve shifts upwards and the T_2 spectrum area increases from 2.26 × 10^3 a.u. to 2.65 × 10^3 a.u. with an increase of 17.51%. Between 500 °C and 600 °C, the T_2 spectrum area increases from 2.65 × 10^3 a.u. to 2.86 × 10^3 a.u. with an increase of 7.75%. Between 600 °C and 700 °C, the curve shifts sharply upwards and the T_2 spectrum area increases from 2.86 × 10^3 a.u. to 4.69 × 10^3 a.u. with an increase of 64.01%. Finally, the curve continues to shift upwards between 700 °C and 800 °C, the T_2 spectrum area increases from 4.69 × 10^3 a.u.to 5.06 × 10^3 a.u. with an increase of 7.81%.

3.5. Pore distribution of thermally treated oil shale rock

Transverse relaxation time (T_2) under a gradient magnetic field mainly includes surface relaxation (T_{2S}), bulk fluid relaxation (T_{2B}), and diffusion relaxation (T_{2D}), and is expressed as

$$\frac{1}{T_2} = \frac{1}{T_{2S}} + \frac{1}{T_{2B}} + \frac{1}{T_{2D}} \quad (1)$$

However, the low-field NMR relaxation measurements T_2 are primarily determined by the surface relaxation (Du et al., 2024; Zhang et al., 2019). Therefore, T_2 can be expressed as

$$\frac{1}{T_2}=\rho_2\frac{S}{V}=\rho_2\frac{a}{r} \quad (2)$$

where, S/V is the surface-to-volume ratio of the pore (μm^{-1}), a is the pore shape constant (2 for cylindrical pores and 3 for spherical pores), ρ2 is surface relaxivity (μm/ms), a material-specific parameter quantifying the relaxation efficiency at the pore-fluid interface. In organic-rich shale, ρ2 is primarily influenced by the interfaces between clay and organic matter, which show minimal variation under static saturation conditions. Prior studies report ρ2 ranges of 0.003 - 0.010 μm/ms for shales, influenced by organic content. Based on previous research recommendations, this paper adopts a surface relaxivity value of ρ2 = 0.007 μm/ms (Zhang et al., 2019). However, it should be noted that the selection of ρ2 has an impact on the calculated pore radius.

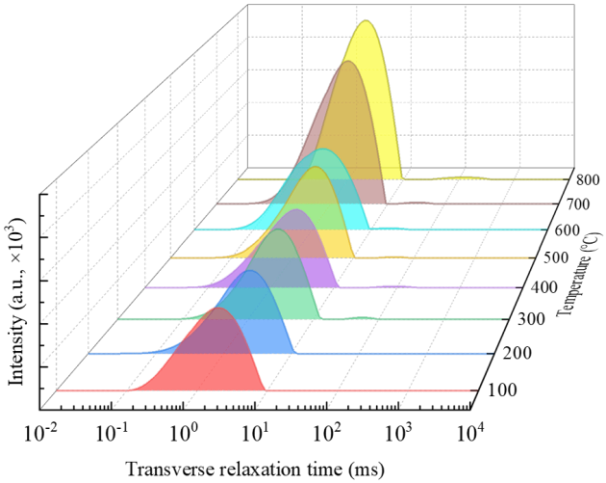

Fig. 8: DT_2 spectra of pore water

Based on the DT_2 spectra of pore water in oil shale presented in Fig. 8, the pore distribution of the oil shale rock can be determined, as illustrated in Fig. 9. Fig. 9 illustrates that the minimum pore radius of oil shale rock is 1.17 nm at 100 °C. Additionally, when the pore radius is 19.17 nm, the porosity component is the maximum (0.25%). It indicates that oil shale has a nanoscale pore structure. Furthermore, the maximum porosity components are observed at temperatures of 200 °C (0.30%), 300 °C (0.34%), 400 °C (0.30%), and 500 °C (0.36%) with corresponding pore radius measuring at 22.04 nm, 29.14 nm, 25.34 nm, and 22.04 nm, respectively. The left wing of the pore distribution curve clearly shifts upward, obviously between 500 °C and 600 °C. It indicates that the porosity of smaller pores varies significantly. At 600 °C and 700 °C, the curve shifts sharply upward, and the maximum porosity component increases from 0.34% to 0.63%. Moreover, the curve demonstrates a continuous upward shift, and the maximum porosity component increases from 0.63% to 0.72% between 700 °C and 800 °C. Additionally, the minimum pore radius of oil shale rock is measured at 1.56 nm at 800 °C, which surpasses that detectable at 700 °C (0.14 nm). This illustrates that not only does the number of pores increase, but also the smaller pores merge into larger ones in shale rock oil at high temperature.

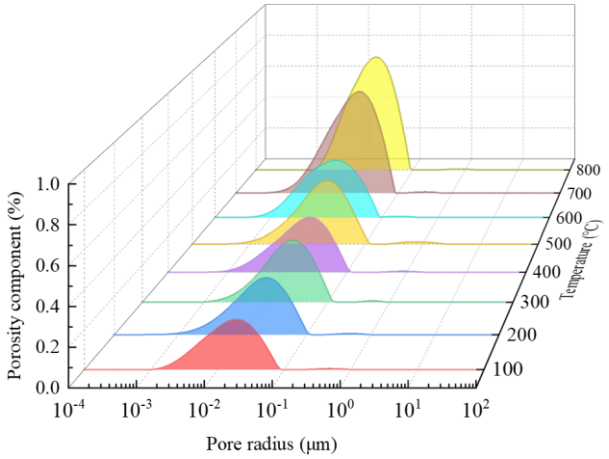

Fig. 9: Pore distribution of oil shale rock based on the DT_2 spectra of pore water

4. Discussion

4.1. Effects of temperature on porosity variation

Porosity is defined as the ratio of pore volume to the total volume of the sample. Pore volume can be determined from the DT_2 spectrum of pore water, which corresponds to the volume of the pore water itself. Fig. 10 illustrates the variation in porosity of oil shale rock as temperature changes. The increase in porosity (ϕ) with temperature (T) was modeled using a modified Boltzmann sigmoidal function as

$$\phi(T)=\frac{\phi_{max}-\phi_{min}}{1+e^{\frac{T-T_c}{k}}}+\phi_{min} \quad (3)$$

where, ϕ_{min} and ϕ_{max} denote the initial porosity at ambient temperature and maximum porosity, respectively. Tc is the critical inflection temperature, and k is the function parameter.

In the present study, ϕ_{min} and ϕ_{max} is fitted as 4.16% and 9.99%, Tc and k are determined as 658.0 °C and 85.0 °C based on the experimental test, respectively. Fig. 10 shows that this model demonstrated excellent agreement with experimental data (R^2 = 0.99), which effectively captures the dual-phase evolution of pore development in oil shale. The porosity of oil shale rock increases slightly from 4.16% to 4.88% when subjected to temperatures between 100 °C and 400 °C, representing an increase of 17.31%. The porosity of oil shale rock increases significantly between 400 °C and 800 °C.

At 400 °C to 600 °C, the porosity of oil shale rock increases from 4.88% to 6.16%, representing a rise of 26.23%. At 600 °C to 800 °C, the porosity of oil shale rock increases from 6.16% to 9.99%, representing an increase of 62.18%.

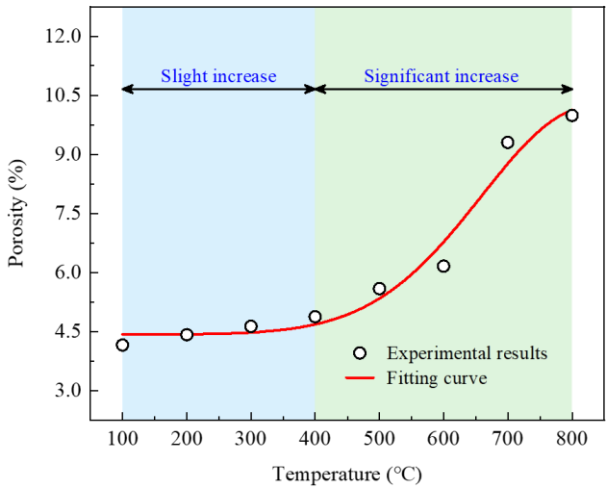

Fig. 10: Porosity variation as temperature increases

4.2. Effects of temperature on variation of porosity change rate

This paper introduces the porosity change rate to further examine the effects of high temperature on the microstructural deterioration of oil shale rock. This rate represents the variation in porosity per unit temperature, as shown in Fig. 11. The porosity change rate of oil shale rock gradually increases slowly from 0.02 × 10^{-3} %/°C to 3.36 × 10^{-3} %/°C at 100 °C to 400 °C, and further indicates that the deterioration of oil shale rock is slow. As the temperature increases to approximately 658 °C, the porosity change rate is the maximum (20.50 × 10^{-3} %/°C), and it is 5.10 times higher than that at 400 °C, further indicating that the deterioration of oil shale rock is accelerated. However, the deterioration of oil shale rock does not continuously increase, especially between 658 °C and 800 °C; the deterioration of oil shale rock is step-down. The above phenomenon indicates that, in addition to the effects of organic matter on the porosity (between 100 °C and 600 °C), the thermal crack is still the dominant cause for the porosity variation (between 600 °C and 800 °C).

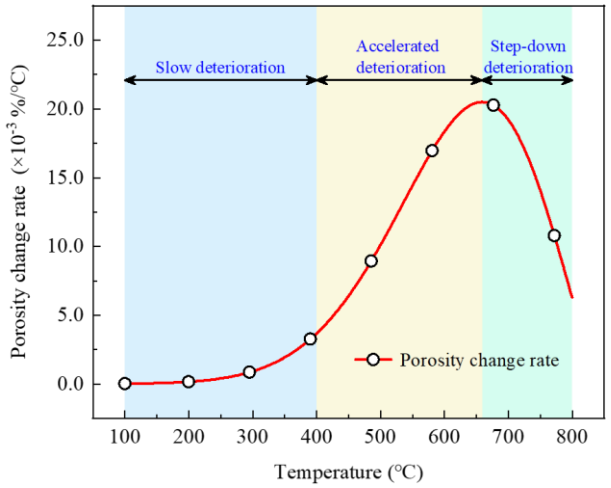

Fig. 11: Porosity change rate variation as temperature increases

According to the results of pore size distribution, porosity and porosity change rate of oil shale at high temperature, the pore structure evolution is governed by the synergistic effects of organic pyrolysis, thermal stress, and mineral phase transitions. Between 100 °C and 400 °C, gradual organic matter pyrolysis generates hydrocarbon products and nanoscale pores (minimum radius: 1.17 nm - 1.56 nm), driving a moderate porosity increase from 4.16% to 4.88% and shifting peak porosity components to larger radii (19.17 nm - 29.14 nm). Between 400 °C and 600 °C, intensified thermal cracking accelerates organic decomposition, expanding pore networks (porosity rises 4.88% to 6.16%) and inducing upward shifts in small-pore distribution curves (between 500 °C and 600 °C), while peak porosity components fluctuate (22.04 nm- 29.14 nm) due to dynamic pore coalescence. Above 600 °C, thermal stress becomes the dominant factor, leading to the propagation of microcracks. This process significantly increases porosity by 62.18% (6.16% to 9.99%) and merges smaller pores (minimum radius increases from 0.14 nm at 700 °C to 1.56 nm at 800 °C). The rate of porosity change peaks at 658 °C (20.50 × 10^{-3} %/°C), marking the transition from organic-driven to fracture-dominated mechanisms.

Based on the research results of this study, the significant porosity increase observed at > 400 °C aligns with the onset of kerogen pyrolysis during underground heating. The DT_2-derived porosity model can analyze pore network development during in-situ conversion processes (ICP), informing optimal heating zone design (e.g., well spacing and target temperature profiles).

The upward shift in pore distribution curves at > 500 °C indicates that pre-heating shale reservoirs to 400 °C - 600 °C could enhance nano-pore connectivity, potentially reducing the fracturing pressure required to initiate cracks. MRI results confirm that thermal cracks propagate parallel to bedding planes. Field operations could leverage this anisotropy by aligning hydraulic fractures with natural thermal crack networks to maximize stimulated reservoir volume.

5. Conclusions

This study investigated the thermal effects on the porosity variation of naturally hydrogen-rich oil shale rock using the DT_2 method, which was employed to differentiate between organic matter and pore water. The conclusions are as follows:

1. The organic matter and pore water in oil shale rock were distinguished by the DT_2 spectrum, which provides a new approach to correct hydrogen signal interference from organic matter, which is a common issue in NMR analysis of oil shale. Based on the DT_2 spectrum, the workflow designed in this paper quantifies organic matter contribution to porosity under high temperature conditions.
2. The porosity of oil shale rock increases slightly when the temperature is below 400 °C. The

porosity of oil shale rock increases significantly between 400 °C and 800 °C. Besides the effects of organic matter on porosity at temperatures ranging from 100 °C to 600 °C, thermal cracking remains the dominant cause of porosity variation between 600 °C and 800 °C.

3. The rate of porosity changes in oil shale rock increases gradually between 100 °C and 400 °C. The temperature increases significantly and then decreases between 400 °C and 800 °C. The most significant effect of high temperature on the porosity of oil shale rock occurs at a temperature of approximate 658 °C in the present study, where the rate of porosity change reaches its maximum.
4. The temperature-dependent porosity thresholds (400 °C and 658 °C in the present study) and DT_2 methodology provide actionable parameters for optimizing in-situ conversion, hydraulic fracturing, and log interpretation in organic-rich shale reservoirs.

Compliance with ethical standards

Conflict of interest

The author(s) declared no potential conflicts of interest with respect to the research, authorship, and/or publication of this article.

References

Alrwashdeh SS (2022). Energy sources assessment in Jordan. Results in Engineering, 13(3): 100329. https://doi.org/10.1016/j.rineng.2021.100329

Bi J, Du C, Zhao Y, Wang CL, Lian SL, and Xiong XH (2023). Characterization of shear behavior and damage mechanism of periodic thermal loading sandstone based on NMR technique. Engineering Geology, 325: 107272. https://doi.org/10.1016/j.enggeo.2023.107272

Burnham AK (2017). Porosity and permeability of Green River oil shale and their changes during retorting. Fuel, 203: 208-213. https://doi.org/10.1016/j.fuel.2017.04.119

Daigle H and Johnson A (2016). Combining mercury intrusion and nuclear magnetic resonance measurements using percolation theory. Transport in Porous Media, 111: 669-679. https://doi.org/10.1007/s11242-015-0619-1

Du M, Yang ZM, Jiang EY et al. (2024). Using digital cores and nuclear magnetic resonance to study pore-fracture structure and fluid mobility in tight volcanic rock reservoirs. Journal of Asian Earth Sciences, 259: 105890. https://doi.org/10.1016/j.jseaes.2023.105890

Fan LF, Gao JW, Du XL, and Wu ZJ (2020). Spatial gradient distributions of thermal shock-induced damage to granite. Journal of Rock Mechanics and Geotechnical Engineering, 12(5): 917-926. https://doi.org/10.1016/j.jrmge.2020.05.004

Feng YJ, Su HJ, Yu LY, Wu C, and Wang H (2023). Mixed mode I-II fracture mechanism of sandstone samples after thermal treatment: Insights from optical monitoring and thermal analysis. Theoretical and Applied Fracture Mechanics, 125: 103883. https://doi.org/10.1016/j.tafmec.2023.103883

Feng ZQ, Jia CZ, Xie XN, Zhang S, Feng ZH, and Cross TA (2010). Tectonostratigraphic units and stratigraphic sequences of the nonmarine Songliao Basin, Northeast China. Basin Research, 22(1): 79-95. https://doi.org/10.1111/j.1365-2117.2009.00445.x

Gautam PK, Verma AK, Sharma P, and Singh TN (2018). Evolution of thermal damage threshold of Jalore granite. Rock Mechanics and Rock Engineering, 51: 2949-2956. https://doi.org/10.1007/s00603-018-1493-2

Ge XM, Chen H, Fan YR, Liu JT, Cai JC, and Liu JY (2017). An improved pulse sequence and inversion algorithm of T_2 spectrum. Computer Physics Communications, 212: 82-89. https://doi.org/10.1016/j.cpc.2016.10.012

He Q, Chen SW, Wang GB, Zuo SY, and Yang FB (2023). Evolution of thermal cracking, temperature distribution and deformation at mineral scale of Beishan granite during heating and cooling. International Communications in Heat and Mass Transfer, 144: 106781. https://doi.org/10.1016/j.icheatmasstransfer.2023.106781

Kang Z, Zhao Y, and Yang D (2020). Review of oil shale in-situ conversion technology. Applied Energy, 269: 115121. https://doi.org/10.1016/j.apenergy.2020.115121

Lei J, Pan BZ, Guo YH, Fan YF, Xue LF, Deng SH, Zhang LH, and Ruhan A (2021). A comprehensive analysis of the pyrolysis effects on oil shale pore structures at multiscale using different measurement methods. Energy, 227: 120359. https://doi.org/10.1016/j.energy.2021.120359

Li JB, Jiang CQ, Wang M et al. (2020). Adsorbed and free hydrocarbons in unconventional shale reservoir: A new insight from NMR T_1-T_2 maps. Marine and Petroleum Geology, 116: 104311. https://doi.org/10.1016/j.marpetgeo.2020.104311

Ma Y, Wang HT, Wang WM, Zhou SX, Ding Y, Pan JL, Fu DL, and Li J (2020). The application of nuclear magnetic resonance T_1-T_2 maps in the research of sedimentary organic matter: A case study of early mature shale with type I kerogen. Journal of Petroleum Science and Engineering, 194: 107447. https://doi.org/10.1016/j.petrol.2020.107447

Rabbani A, Baychev TG, Ayatollahi S, and Jivkov AP (2017). Evolution of pore-scale morphology of oil shale during pyrolysis: A quantitative analysis. Transport in Porous Media, 119: 143-162. https://doi.org/10.1007/s11242-017-0877-1

Rossi E, Kant MA, Madonna C, Saar MO, and Rudolf von Rohr P (2018). The effects of high heating rate and high temperature on the rock strength: Feasibility study of a thermally assisted drilling method. Rock Mechanics and Rock Engineering, 51: 2957-2964. https://doi.org/10.1007/s00603-018-1507-0

Saif T, Lin Q, Butcher AR, Bijeljic B, and Blunt MJ (2017). Microstructural imaging and characterization of oil shale before and after pyrolysis. Fuel, 197: 562-574. https://doi.org/10.1016/j.fuel.2017.02.030

Tian H, He K, Huangfu YH, Liao FR, Wang XM, and Zhang SC (2024). Oil content and mobility in a shale reservoir in Songliao Basin, Northeast China: Insights from combined solvent extraction and NMR methods. Fuel, 357: 129678. https://doi.org/10.1016/j.fuel.2023.129678

Wang CG, Zhang JD, Chen JG, Zhong RZ, Cui GL, Jiang YJ, Liu WT, and Chen ZW (2021). Understanding competing effect between sorption swelling and mechanical compression on coal matrix deformation and its permeability. International Journal of Rock Mechanics and Mining Sciences, 138: 104639. https://doi.org/10.1016/j.ijrmms.2021.104639

Wang L, Zhao Y, Yang D, Kang Z, and Zhao J (2019). Effect of pyrolysis on oil shale using superheated steam: A case study on the Fushun oil shale, China. Fuel, 253: 1490-1498. https://doi.org/10.1016/j.fuel.2019.05.134

Wu ZJ, Zhou YY, Weng L, Liu QS, Xiao Y, Hu MS, Steefel C, and Rutqvist J (2020). Investigation of thermal-induced damage in fractured rock mass by coupled FEM-DEM method. Computational Geosciences, 24(5): 1833-1843. https://doi.org/10.1007/s10596-020-09970-5

Yang RF, Wang K, Zhang L, Sun H, Zhang K, and Ma JS (2019). Pore-scale simulation of shale oil flow based on pore network

model. Fuel, 251: 683-692. https://doi.org/10.1016/j.fuel.2019.03.083

Yuan SH, Sun Q, Li PF, Geng JS, and Zhang H (2022). Fracture properties and dynamic failure of three-point bending of yellow sandstone after subjected to high-temperature conditions. Engineering Fracture Mechanics, 265: 108366. https://doi.org/10.1016/j.engfracmech.2022.108366

Zhan HL, Qin FK, Chen ST, Chen R, Meng ZH, Miao XY, and Zhao K (2022). Two-step pyrolysis degradation mechanism of oil shale through comprehensive analysis of pyrolysis semi-cokes and pyrolytic gases. Energy, 241: 122871. https://doi.org/10.1016/j.energy.2021.122871

Zhang GL, Regaieg M, Blunt MJ, and Bijeljic B (2023). Primary drainage and waterflood capillary pressures and fluid displacement in a mixed-wet microporous reservoir carbonate. Journal of Hydrology, 625: 130022. https://doi.org/10.1016/j.jhydrol.2023.130022

Zhang SL, Yan JP, Hu QH, Wang J, Tian TH, Chao J, and Wang M (2019). Integrated NMR and FE-SEM methods for pore structure characterization of Shahejie shale from the Dongying Depression, Bohai Bay Basin. Marine and Petroleum Geology, 100: 85-94. https://doi.org/10.1016/j.marpetgeo.2018.11.003

Zheng YL, Ma ZJ, Gong QM, Zhang PH, Zhao XB, and Li JC (2022). Heating-dominated fracturing of granite by open-ended microwave: Insights from acoustic emission measurement. Rock Mechanics and Rock Engineering, 55: 4577-4589. https://doi.org/10.1007/s00603-022-02887-8